RSC Advances

ROYAL SOCIETY OF CHEMISTRY

www.rsc.org/advances

Synthesis and thermal expansion property of $(Ba_{0.5}Sr_{0.5})_{0.9}Bi_{0.1}Co_{0.8}Fe_{0.2}O_{3-\delta}$ cathode materials for IT-SOFCs

Dechuan Li[1*], Guangping Zhu[1],Yong-xing Zhang[1], Yijun Yang[1], Changbao Han[2]

[1] School of Physics & Electronic Information, Huaibei Normal University, Huaibei, 235000, China

[2]Beijing Institute of Nanoenergy and Nanosystems, Chinese Academy of Sciences, Beijing, 100083, China

Abstract

Perovskite cathode material, $(Ba_{0.5}Sr_{0.5})_{0.9}Bi_{0.1}Co_{0.8}Fe_{0.2}O_{3-\delta}$ (BSBCF-0.1), was synthesized by a combined citrate-EDTA complexing method for intermediate temperature solid oxide fuel cells. The Bi element was successfully added to the perovskite structure. A small amount of Bi element could enter into the A-site of the perovskite structure, and Bi ionic would enter the B-site of BSCF structure when the concentration is larger than 0.1. Thermal expansion coefficient (TEC) of BSBCF-0.1 is lower than that of undoped BSCF in the working temperature range. The decreased TEC of BSBCF may be more suitable for the thermal compatibility of cell components. The maximum power density is 220, 270 $mWcm^{-2}$ at 600, 650^{o}C, respectively. The result suggested that the perovskite BSBCF material could be considered as the cathode for IT-SOFCs.

Keywords: Solid oxide fuel cells; BSCF; Stabilization; Polarization resistance

1. Introduction

Solid oxide fuel cells (SOFCs), as a new kind of generating equipment, have

attracted much attention due to its high-efficiency, low-pollution, modular design and fuel flexibility. Recently, many efforts have been made to reduce the working temperature of SOFCs in order to avoid a series of problems such as the high-cost metallic interconnectors, chemical and thermal compatibility of cell components and performance degradation [1-4]. However, SOFCs operating at a relatively lower temperature needs a special cathode material with relatively higher conductivity and proper thermal expansion coefficient[5,6]. The perovskite structure (ABO_3) $Ba_{0.5}Sr_{0.5}Co_{0.8}Fe_{0.2}O_{3-\delta}$ (BSCF), with the mixed ionic and electronic conductivity, was selected as a candidate cathode material owing to its high catalytic activity for oxygen reduction and good oxygen ion permeability [7, 8]. As is well known, electrochemical activity is deteriorated abruptly when the temperature is decreased for SOFCs, and cell life has closed relationship with the compatibility between cathode and electrolyte materials. However, the larger thermal expansion coefficient (TEC) of BSCF will cause the thermally incompatibility with electrolyte. The drawbacks have been attempted to resolve by the substitution of A- or B- site cations in ABO_3 structure. Meng et al reported Zr-substituted BSCF perovskite cathode material, $Ba_{0.5}Sr_{0.5}(Co_{0.6}Zr_{0.2})Fe_{0.2}O_{3-\delta}$, has excellent thermal stability even though an increased area specific resistance (ASR) than that of BSCF [9]. Chemical stability for BSCF has also been improved by adding the Ti in B-site of the ABO_3 perovskite oxide [10]. The rare earth ions, such as Sm^{3+} [11], Gd^{3+} [12], Nd^{3+} [13] were also added into A-site cations of BSCF to elevate the electrical conductivity, but increased the TEC of BSCF and degenerated the thermally incompatibility between the cell's components. It is

reported that Bi could be doped into $SrFeO_{3-\delta}$ perovskite structure, and the material is compatible with the Sm doped Ceria electrolyte for the low TEC [14]. Considering the Bi could be introduced to the perovskite structure, therefore, Bi was selected to reduce the TEC and increase the conductivity for BSCF.

In this paper, Bi was introduced to the perovskite oxide of BSCF to form a new $(Ba_{0.5}Sr_{0.5})_{0.95}Bi_{0.05}Co_{0.8}Fe_{0.2}O_{3-\delta}$ cathode material for intermediate temperature SOFCs. The major aim is to develop a special cathode material with low TEC and enhanced electrical performance. The phase structure, TECs and electrochemical properties were also discussed.

2. Experiment

$(Ba_{0.5}Sr_{0.5})_{1-x}Bi_xCo_{0.8}Fe_{0.2}O_{3-\delta}$ (x=0, 0.1, 0.125, 0.15) (noted as BSCF(x=0) and BSBCF-x) powders were synthesized by a glycine-nitrate combustion process [15]. The analytical reagents, $Ba(NO_3)_2$, $Sr(NO_3)_2$, $Bi(NO_3)_3{\cdot}6H_2O$, $Co(NO_3)_2{\cdot}6H_2O$ and $Fe(NO_3)_3{\cdot}9H_2O$ were used as starting materials. All the nitrate salts were dissolved in the EDTA (ethylenediaminetetraacetic acid) and NH_4OH solution under stirring at 80^{o}C. Then the citric acid solution was added, which was used as a complexing reagent. The molar ratio of metal ions: EDTA: citric acid was fixed at 1:1:1.5. The mixed solution was stirred and heated at 120^{o}C for 48 h. The BSBCF precursor was sintered at 800^{o}C for 12h, then 1050^{o}C for 12 h to obtain the final powder. The powders were compacted into a cylinder with a diameter of 13mm under 400Mpa uniaxial pressing. The compacts were sintered at 1100 ^{o}C for 6h with a heating and cooling rate of 5 ^{o}C/min. Two faces of dense samples were polished to parallel by

sand paper for TEC measurement. The approximate dimensions of BSCF, BSBCF-0.1, BSBCF-0.125, BSBCF-0.15 samples were about Φ11×7, Φ11×5, Φ11×3，Φ11×6 mm^3 respectively. Densities were exceed 94% of the theoretical value as measured by the Archimedes method.

In the cell fabrication, the dense electrolyte $Ce_{0.82}La_{0.18}O_{2-\delta}$(LDC) was prepared by solid-state reaction similar to our previous work [16]. Anode materials were made of 80 wt% LDC-NiO (with a ratio of 60 wt%:40 wt%) and 20 wt.% starch, then mixed with appropriated terpineol to form mixed slurry. Anode slurry was painted on one side of dense LDC electrolyte, and then the bilayer was sintered at 1400 °C for 6 h. Four kinds of ground cathode powders (60%) were dispersed homogeneously into terpineol (40%) to obtain the cathode slurry. The mixed cathode slurry was painted on the other side of LDC supporter and sintered at 1100°C for 4 h, and finally to form a single cell of BSBCF-*x*|LDC|NiO-LDC. Fuel cell has the properties of electrolyte thickness of ~1mm, cathode thickness of 80μm, and anode thickness of 0.7mm. The single fuel cells with an effective cathode area of 0.45cm^2 were prepared. On the cell performance test, the cathode was exposed to air, and the anode side was exposed to 3% H_2O+humidified H_2 at a flow rate of 50 ml min^{-1}.

The crystal structures of the powders were characterized by X-ray diffraction (XRD) using an X'pert PRO diffractometer and Cu Kα radiation in the 2θ range of 10-80°. Scanning electron microscopy (SEM) and energy dispersive spectrometry (EDS) were employed to examine the morphology and element distribution of sample. The linear thermal expansion coefficient was measured on the thermal expansion apparatus

(LINSEIS DIL L76) using the quartz as the reference material with a heating rate of 5 ^{o}C/min from room temperature to 800 ^{o}C. The performances of the fuel cells were determined by a PARSTAT 2273 electrochemical workstation (Princeton, USA) at 600^{o}C and 650^{o}C.

3. Results and discussion

3.1 Crystal structure

Fig. 1 shows the X-ray diffraction patterns of BSBCF-x(x=0, 0.1, 0.125, 0.15) samples. It can be observed that all the samples possess the cubic perovskite-type structure similar to Niedrig [17]. The lattice parameters of BSBCF-x were calculated by jade 6.0. The calculated parameters were shown in **Table 1** . The calculation lattice of BSCF agrees well with the values determined by references[13, 18]. From the X-ray diffraction patterns, the main diffraction peaks of BSBCF-x shift gradually to higher angles at low Bi doping concentration compared to that of the perovskite BSCF oxide. In right Fig. 1, the amplified image shows an obvious shift of 2θ. The reason for the change was due to the Bi^{3+} successful introduction into the lattice of BSCF. The pre-sintering temperature of 800^{o}C is the key factor to reduce the volatilization for doping Bi^{3+} because Bi could be volatile when the sintering temperature high than the melting point of cubic Bi_2O_3 (825^{o}C) in air environment [19].

With the substitution of the larger Ba^{2+} (0.175nm) and Sr^{2+} (0.158nm) for smaller Bi^{3+} (0.103nm) in A-site [20, 21], the lattice volume of BSCF cathode decreased. As the substitution concentration increasing, the reducing rate of the lattice volume slow

down compared to BSBCF-0.1 for BSBCF-0.125. The lattice volume and the average ionic radius accordingly increased when the addition further increased, the redundancies of Bi^{3+} entered into the B-site of the perovskite structure [22]. The diffraction peaks move to the direction of small angle of BSBCF-0.15. It indicates that the element of Bi could enter the B-site of BSCF when the concentration of *x* is larger than 0.1.

3.2 SEM-EDS analysis

To illustrate the distribution state of elements, SEM-EDS micro-region composition analysis was taken for the unground BSBCF-*x* powders. For comparative analysis, BSCF, BSBCF-0.1 and BSBCF-0.15 were performed. As is shown in Fig. 2(a), (b) and (c), the powders is easily sintered as the Bi concentration increasing. The grains of large size are observed. To study the distribution of element, the element mapping mode was selected at random on the surface of three powders. The element composition of BSBCF-*x* were calculated and summarized in Table 2. The chemical composition of BSCF is as follows: Ba 7.34%, Sr 5.80%, Co 7.75%, Fe 2.09%. The BSBCF-0.1 exhibits a composition of Ba 10.30%, Sr 11.10%, Bi 1.64%, Co 17.53%, Fe 5.28%. The ratios of A-site to B-site of two (BSCF and BSBCF-0.1) perovskite oxides are closed to 1. In the EDS spectrums (Fig. 2(d)), it is easy to distinguish the peak position of Bi element between BSCF and BSBCF-0.1 at 2.42~2.53 KeV. The characteristic X-Ray energies of all elements were shown in Table 3. The peak of Bi is also obvious in BSBCF-0.15 spectrum. However, the total concentration of Ba and Sr closes to the sum of Sr and Co for BSBCF-0.15. Whatever the Bi was count to the

A-site or B-site, it will change the balance of stoichiometric ratio. Therefore, we conclude that Bi could enter the A-site of the perovskite structure when the concentration is smaller than 0.1. Otherwise, it will enter B-site of the perovskite structure.

3.3 Thermal expansion analysis

Fig. 3(a) shows the thermal expansion behaviors of BSBCF-*x*(x=0, 0.1, 0.125, 0.15) samples measured in the range from room temperature to 800^{o}C in air. The TEC of BSCF is similar to the results reported by Li[13]. High densities of the sample minimize the influence of pore in our TEC test. The average TECs of BSBCF-*x* were shown in Table 4. It is found that the TEC of BSBCF-0.1 is lower than that of BSCF. The lower TEC of cathode indicates the better integration of BSBCF-0.1 to LDC electrolyte. Even though the average TEC is similar, but the curve is significantly different, especially under working temperature below 650 ^{o}C. The relative length variation is much less for BSBCF-0.1 than that of BSCF especially over 450^{o}C. The TEC slightly reduces with a little content of Bi^{3+} addition. It could be mainly attributed to the decreasing of the average ionic radius. When the addition of Bi^{3+} is further increased, however, the relative change is much more steadily in the range of about 250^{o}C to 450^{o}C. The material expansion is large than BSCF below 500^{o}C and more stability at the high temperature. One of the reasons is some of Bi^{3+} entered into the B-site of the perovskite oxide. The additional oxygen vacancies can be generated by A-site deficiency [23]. Another is the average ionic radius could be enlarged by the substitution of Bi^{3+} (0.103nm) for Co^{4+} (0.053) and Fe^{4+} (0.059) [22]. When the

temperature is elevated, the lattice oxygen becomes more active, and released from the lattice. The variable tendency of TEC for BSBCF-*x* presents the clear change in Fig. 3(b). The turning points of the thermal expansion curve gradually shift by oxygen emission. It indicates that the stabilization of BSCF cathode material with Bi^{3+} substitution is increased steadily with a small value of TEC and less variation from room temperature to the working temperature for SOFCs.

3.4 Electrochemical behaviors

In our experiment, we found that the relative density of cathode has something to do with the addition of Bi. Cathode materials sintered more easily while the volatile Bi was added steadily. High density means the low gas diffusion. In order to evaluate the electrochemical performance, low TEC cathode material of BSBCF-0.1 was selected to fabricate the cell of BSBCF-0.1|LDC|Ni+LDC, and the cell of BSCF|LDC|Ni+LDC was also fabricated for comparison. Fig 4 shows the microstructural of the fracture surface of BSBCF-0.1 cathode sintered at 1100^{o}C on LDC electrolyte. From the picture, it can be clearly seen that the electrode has a porous structure. The optimized temperature for the cell fabrication was found to be between 1000 and 1150 ^{o}C.

As is illustrated in Fig. 5, the electrochemical performances (I—V and power density curves) of the single fuel cell were measured at 600^{o}C and 650^{o}C. The open circuit voltage (OCV) is about 0.82V at the temperature of 600^{o}C for two single cells corresponding to the CeO_2-base electrolyte. A slight decrease on the OCV has been found as the work temperature elevated.

From the curve of output power density, the maximum power densities were about 220, 270 $mWcm^{-2}$ at 600, 650^{o}C, respectively, for the cell with the BSBCF-0.1 cathode (Fig. 5(a)). While the peak power densities were 100 $mWcm^{-2}$ (600^{o}C) and 130 $mWcm^{-2}$ (650^{o}C) for the cell constructed with the BSCF cathode (Fig. 5(b)). The output power density is large than Zr-doped $Ba_{0.5}Sr_{0.5}(Co_{0.6}Zr_{0.2})Fe_{0.2}O_{3-\delta}$ cathode material for SOFC(139 $mWcm^{-2}$ at 650^{o}C) [9]. However, the power density is low than the electrode-supported fuel cell because of the thin electrolyte [7]. Therefore, the electrode-supported structure would be taken to enhance the cell performance in the future work.

The relatively lower output power density is related to some reasons: one of the reasons is the mixed conductive of CeO_2-base electrolyte increased the internal electric energy consumption of the cell. Another is the low current density is possibibly unfavourable to high power density. Fig. 6 shows the electrochemical impedance spectra of BSCF and BSBCF-0.1 fuel cells at 650^{o}C. The standard impedance spectra of cell consist of three parts: the real axis intercept, two arcs and Warburg resistance. The curve intercept with the real axis at high frequence is attributed to the full cell ohm resistance. The two arcs mainly consist of cathode electrochemical reaction. Anode reaction arc always buries into a larger arc because of its higher activity than that of cathode. Warburg resistance is related to the diffusion of gas in the electrode. According to the impedance spectra, ohm resistance values were almost the same between BSCF and BSBCF-0.1. However, the BSCF fuel cell has a larger flat arc, which consists of the difusion and reaction of gas in the electrode, than

that of BSBCF-0.1. Large resistance depressed the efficiency of fuel cell. Moreover, the low current densities were observed for two cells constructing by the BSCF or BSBCF-0.1 cathode materials, respectively. However, the maximum output power density of the cell constructed by the BSBCF-0.1 cathode material is better than BSCF. It indicates that the electrochemical reaction activity of BSCF cathode was enhanced by the Bi addition. The whole effect could be mainly related to the increasing density of oxygen vacancies per unit by the addition of small ionic radio of Bi^{3+} to A-site of perovskite structure [21]. The effect of doped Bi ion on the oxygen vacancies resulted from the lattice shirking for BSBCF-0.1. Ding et al ascribed the better electrochemical performance of A-site La doped perovskite material to the improved oxygen adsorption and desorption [24].

4. Conclusion

A new series of cathode materials $(Ba_{0.5}Sr_{0.5})_{1-x}Bi_xCo_{0.8}Fe_{0.2}O_{3-\delta}$ (x=0, 0.1, 0.125, 0.15) have been prepared by a citric-nitrate process. The volatile Bi was successfully added to the perovskite oxide of BSCF. While the content of Bi less than 0.1, the element could mainly enter the A-site of the perovskite structure. The average small ionic radius strengthened the stability of BSBCF-0.1 lattice with the small expansion. As the content further increasing, the Bi element would enter the B-site. The temperature of oxygen loss is steadily elevated as the Bi content increased. A relative lower thermal expansion coefficient of BSBCF-0.1 Cathode material would be more suitable for ceria-base electrolyte. And the output power density of the cell is 270 $mWcm^{-2}$ at 650^oC constructed with BSBCF-0.1 cathode. Therefore, the BSBCF-0.1 is

a promising cathode material for IT-SOFCs.

Acknowledgement

This work was financially supported by the National Natural Science Foundation of China (51302102) and Huaibei Normal University Youth Research Project (Grant No: 2014xq001).

References

[1] T. Hibino, A. Hashimoto, T. Inoue, J. I. Tokuno, S. I. Yoshida, M. Sano, Science, 2000,288, 2031-2033.

[2] E. D. Wachsman, K. T. Lee. Science, 2011,334,935-939.

[3] A. Ecija, K. Vidal, A. Larrañaga, A. Martínez-Amesti, L. Ortega-San-Martín, M.I. Arriortua, Solid State Ionics. 2013,235,14-21.

[4] W. Araki, J. Malzbender, Solid State Ionics. 2013,233 ,67-72.

[5] T. Wei, Y. H. Huang, L. Jiang, J. H. Yang, R. Zeng, J. B. Goodenough, RSC Adv., 2013, 3, 2336-2340.

[6] S. Park, S. Choi, J. Shin, G. Kim, RSC Adv., 2014, 4, 1775-1781.

[7] Z. Shao, S.M. Haile, Nature, 2004, 431, 170-173.

[8] F.S. Baumann, J. Fleig, H.U. Habermeier, J. Maier, Solid State Ionics. 2006, 177 , 3187-3191.

[9] X. Meng, B. Meng, X. Tan, N. Yang, Z. F. Ma, Mater. Res. Bull. 2009, 44, 1293-1297.

[10] L. Bi, E. Fabbri, E. Traversa, Solid State Ionics. 2012, 214, 1-5.

[11] S. Li, Z. Lü, B. Wei, X. Huang, J. Miao, G. Cao, R. Zhu, W. Su, J. Alloy. Compd. 2006, 426, 408-414.

[12] Z. Li, B. Wei, Z. Lü, Y. Zhang, K. Chen, J. Miao, W. Su, Ceram. Int. 2012, 38, 3039-3046.

[13] S. Li, Z. Lü, X. Huang, W. Su, Solid State Ionics. 2008,178, 1853-1858.

[14] Y. Niu, W. Zhou, J. Sunarso, L. Ge, Z. Zhu, Z. Shao, J. Mater Chem. 2010, 20, 9619-9622.

[15] Z. Shao, W. Yang, Y. Cong, H. Dong, J. Tong, G. Xiong, J. Membrane Sci. 2000, 172, 177-188.

[16] D. C. Li, M. J. Chao, J. M. Yu, M. Y. Li, J. J. Zhang, E. J. Liang, Mater. Lett. 2012, 86,171-173.

[17] C. Niedrig, S. Taufall, M. Burriel, w. menesklou, S. F. Wagner, S. Baumann, E. Ivers-tiffee. Solid State Ionics, 2011, 197, 25-31.

[18] S. McIntosh, J. F. Vente, W. G. Haije, D. H. A. Blank, H. J. M. Bouwmeester. J. Chem. Mater., 2006, 18, 2187-2193.

[19] A. M. Azad, S. Larose, S. A. Akbar, J. Mater. Sci. 1994, 29, 4135-4151.

[20] S. V. Moharil, B. S. Nagrare, S. P. S. Shaikh, Int. J. Hydrogen Energ. 2012, 37, 5208-5215

[21] Y. J. Niu, W. Zhou, J.Sunarso, L. Ge, Z. Zhu, Z. Shao, J. Mater. Chem. 2010, 20, 9619-9622.

[22] Z. P. Shao, G. X. Xiong, Y. Cong, W. S. Yang, J. Membrane Sci., 2000, 164, 167-176.

[23] W. L Li, K. Lu, Z. B. Xia, J. Power Sources, 2013, 237, 119-127.

[24] X. F. Ding, X. Kong, J. J. Jiang, C. Cui, X. X. Guo, Mater. Res. Bull., 2010, 45, 1271-1277.

Captions

Fig. 1 X-ray diffraction patterns for BSBCF-*x* (*x*=0, 0.1, 0.125, 0.15).

Fig. 2 SEM-EDS micrographs of the BSBCF-x powders: (a) BSCF; (b) BSBCF-0.1; (c) BSBCF-0.15; (d) a representative EDS spectrums of BSBCF-x powders.

Fig. 3 Thermal expansion curves (a) and TECs (b) for BSBCF-*x*(*x*=0, 0.1, 0.125, 0.15).

Fig. 4 SEM micrograph of the intersection of BSBCF-0.1 cathode on LDC electrolyte

Fig. 5 Cell voltage and Power density as functions of Current density from Cathode|LDC|Ni-LDC fuel cells. Cathode (a): BSCF; Cathode (b): BSBCF-0.1. Measured in humidified H_2 and air at 600^{o}C, 650^{o}C (Anode H_2 flow rate=50ml min^{-1}, Cathode exposed to air).

Fig. 6 Electrochemical impedance spectra of BSCF and BSBCF-0.1 fuel cells at 650^{o}C.

Table 1 The lattice parameters of $(Ba_{0.5}Sr_{0.5})_{1-x}Bi_xCo_{0.8}Fe_{0.2}O_{3-\delta}$

Table 2 Composition of the detected elements of the random area on the surfaces of the BSBCF-*x* samples (Fig. 2(a), (b), (c)).

Table 3 Characteristic X-Ray Energies of elements (Ba, Sr, Co, Fe, Bi, O).

Table 4 TEC values of $(Ba_{0.5}Sr_{0.5})_{1-x}Bi_xCo_{0.8}Fe_{0.2}O_{3-\delta}$

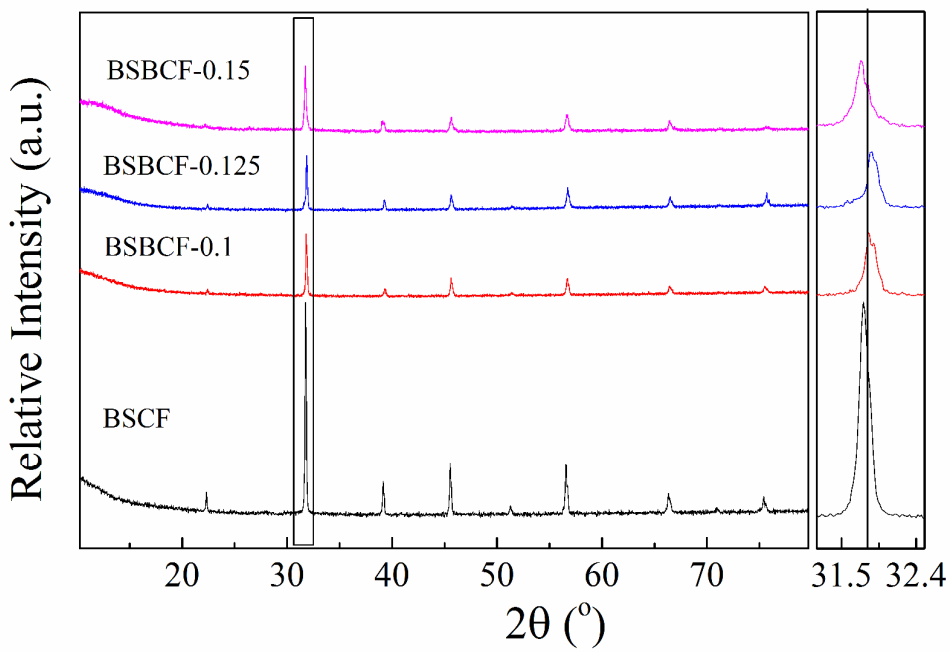

Fig. 1

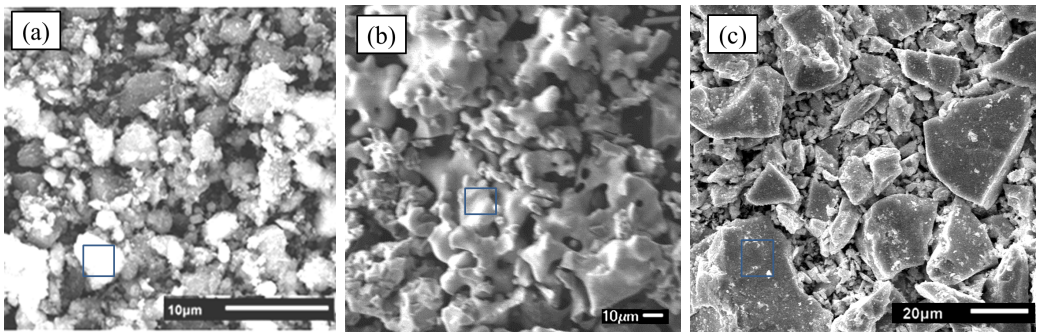

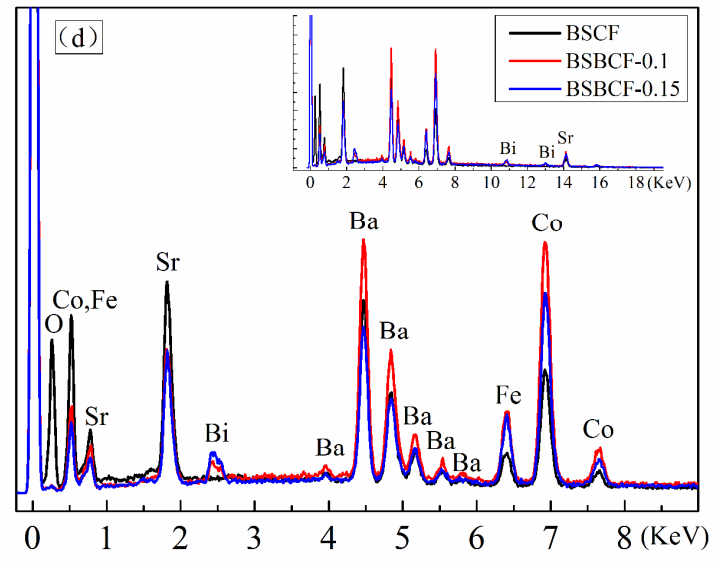

Fig. 2

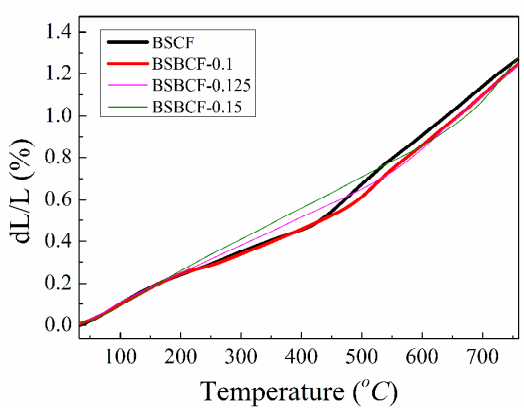

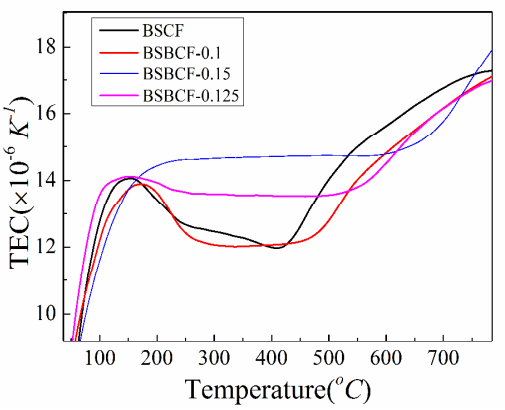

Fig. 3(a) **Fig. 3(b)**

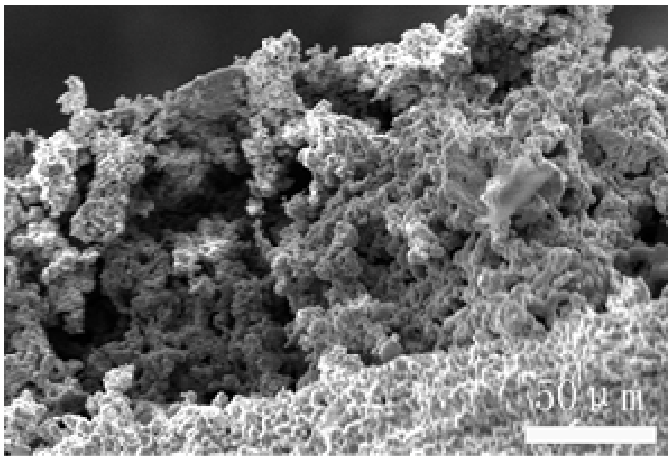

Fig 4

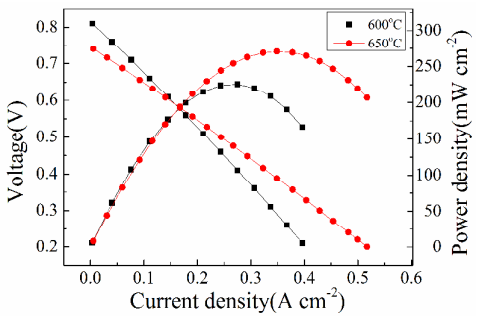

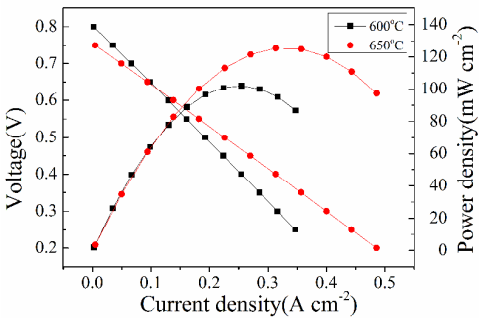

Fig. 5(a) **Fig. 5(b)**

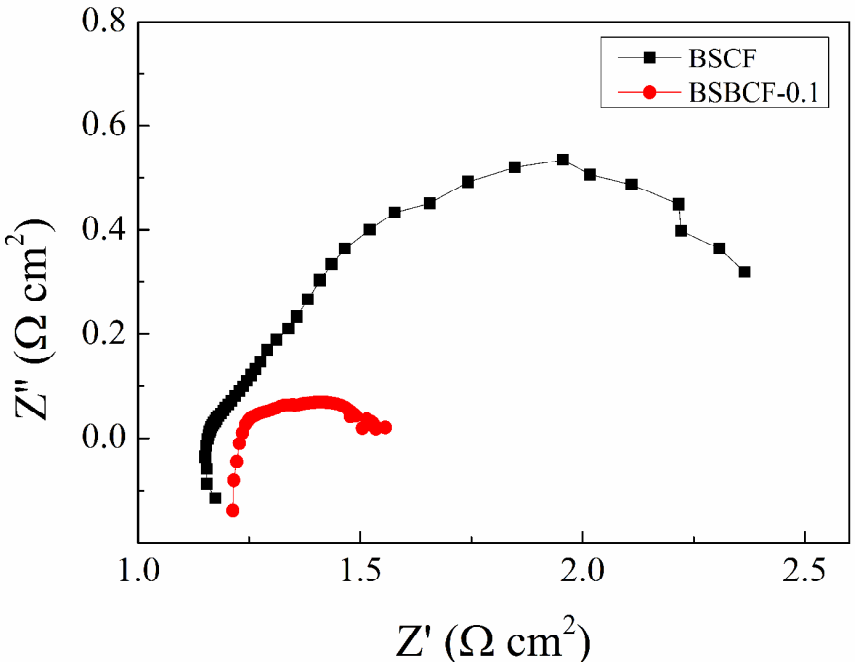

Fig. 6

Table 1

***x* in** $(Ba_{0.5}Sr_{0.5})_{1-x}Bi_xCo_{0.8}Fe_{0.2}O_{3-\delta}$	**Structure**	**A(Å)**
0	Cubic	4.0199
0.1	Cubic	3.9980
0.125	Cubic	3.9824
0.15	Cubic	4.0701

Table 2

Element	Atomic (%)		
	BSCF	BSBCF-0.1	BSBCF-0.15
O K	77.02	54.15	54.90
Fe K	2.09	5.28	5.37
Co K	7.75	17.53	16.28
Sr K	5.80	11.10	12.12
Ba L	7.34	10.30	9.09
Bi L		1.64	2.25
total	100	100	100

Table 3

Element	Characteristic X-Ray Energies **(KeV)**					
Ba	3.945	4.466	4.828	5.157	5.531	5.797
Sr	1.582	1.649	1.807	14.165	15.836	16.085
Co	0.678	0.694	0.776	6.93	7.65	
Fe	0.628	0.705	6.404	7.058		
Bi	1.883	2.424	2.526	2.736	9.42	10.839
O	0.525					

Table 4

Sample	TEC ($10^{-6}K^{-1}$)		Reference
	25-450 °C	25-800 °C	
BSCF	12.61	17.85	This study
BSBCF-0.1	12.16	17.46	This study
BSBCF-0.125	13.53	17.06	This study
BSBCF-0.15	14.72	18.53	This study
BSCF	--	19.7	[13]
BSCF	--	19	[18]